Computers and Geotechnics 146 (2022) 104695

Contents lists available at ScienceDirect

Computers and Geotechnics

journal homepage: www.elsevier.com/locate/compgeo

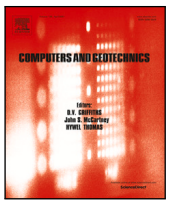

Research paper

Fabric response to stress probing in granular materials: Two-dimensional, anisotropic systems

Chaofa Zhao [a,*], Niels P. Kruyt [a], Mehdi Pouragha [b], Richard Wan [c]

[a] Department of Mechanical Engineering, University of Twente, The Netherlands
[b] Civil and Environmental Engineering Department, Carleton University, Canada
[c] Civil Engineering Department, University of Calgary, Canada

ARTICLE INFO

Keywords:
Granular material
Fabric evolution
Stress/strain probing
DEM simulation

ABSTRACT

The microstructure of granular materials has a significant influence on their macroscopic quasi-static strength and deformational behaviour. This microstructure is often quantified by a second-order fabric tensor that describes the primary orientational statistics of interparticle contacts. Here, it is investigated how the fabric tensor changes when samples are subjected to small (strain) loadings with different 'directions', i.e. probes. This is accomplished by the analysis of extensive sets of Discrete Element Method (DEM) simulations for various anisotropic, pre-peak two-dimensional samples, where both in-plane (i.e. coaxial with the current stress and fabric tensor) and out-of-plane, noncoaxial probes are considered. The results of DEM simulations show that the in-plane and out-of-plane fabric responses are effectively decoupled, i.e. they are only dependent on the in-plane and out-of-plane strain increment, respectively. The out-of-plane fabric increment is proportional to the out-of-plane strain increment whereas the in-plane fabric increment is linearly dependent on the in-plane strain increment. An accurate theoretical description (with a modest number of model parameters) has been developed that describes the fabric response to the imposed, in-plane as well out-of-plane, strain increments for the considered systems.

1. Introduction

Granular materials consist of particles and voids at the micro-scale. Their arrangement, or microstructure, is important to their quasi-static behaviour at the continuum, macro-scale in terms of shear strength and dilatancy (Reynolds, 1885; Rowe, 1962; Rothenburg and Bathurst, 1989; Kruyt and Rothenburg, 2016, 2019), as has been shown both experimentally (Oda, 1972; Yoshimine et al., 1998) and by Discrete Element Method (*DEM* for short) (Cundall and Strack, 1979) simulations (Thornton and Barnes, 1986; Kruyt, 2012; Wang et al., 2017; Shi and Guo, 2018a,b; Wang et al., 2020). This microstructure is often quantified by a second-order fabric tensor (Oda, 1972; Satake, 1978) that represents an average of the dyadic product of a micro-scale vector. Anisotropy of the fabric tensor may originate from depositional or stress-induced processes.

Various types of fabric tensors that differ in the involved micro-scale vectors have been developed in the literature. Examples of widely-used fabric tensors are: the contact normal-based tensor (Satake, 1978; Oda, 1982; Hu et al., 2021), the branch vector-based tensor (Christoffersen et al., 1981), the void vector-based tensor (Tsuchikura and Satake, 2001; Li and Li, 2009; Theocharis et al., 2017a), and the particle orientation vector-based tensor (Oda, 1972; Yang et al., 2008). In this study, the contact normal-based fabric tensor is adopted, which is attractive since force transmission occurs at contacts.

Fabric and its evolution have been studied experimentally (primarily by x-ray tomography measurements, see for example Imseeh et al. (2018), Viggiani and Tengattini (2019), Wiebicke et al. (2020) and Zhao et al. (2021)) and by DEM simulations (see for example Kruyt (2012), Fu and Dafalias (2011), Zhao and Guo (2013) and Yang and Wu (2016)). Such DEM simulations are very convenient for studies on fabric, since very detailed information on particle positions and contacts is readily available that can be used to accurately quantify fabric tensors. Mechanisms of fabric evolution have been studied by Kuhn (2010) and Kruyt (2012). The three mechanisms that have been quantified in Kruyt (2012) are contact disruption, contact creation and contact reorientation.

The importance of fabric to the behaviour of granular materials suggests that it should be appropriately included in (advanced) continuum constitutive relations (Pietruszczak and Pande, 2001; Gao et al., 2014; Yang et al., 2018; Petalas et al., 2019) that describe the behaviour at the macro-scale. Since the fabric tensor generally is not constant,

* Correspondence to: Department of Civil Engineering, Zhejiang University, China.
E-mail address: chaofa.zhao@zju.edu.cn (C. Zhao).

https://doi.org/10.1016/j.compgeo.2022.104695
Received 26 August 2021; Received in revised form 18 February 2022; Accepted 22 February 2022
Available online 11 March 2022
0266-352X/© 2022 The Author(s). Published by Elsevier Ltd. This is an open access article under the CC BY license (http://creativecommons.org/licenses/by/4.0/).

an evolution 'law' is required. Such fabric evolution laws have been fairly extensively studied in the literature, mainly for predicting the evolution of fabric anisotropy for specific loading paths, such as triaxial or isobaric paths, see for instance Li and Dafalias (2012), Zhao and Kruyt (2020), Wang et al. (2020) and Zhao et al. (2021). An overview of different classes of such relations is presented in Zhao and Kruyt (2020).

A framework for conditions at the critical state that must be satisfied by such evolution laws is provided by the Anisotropic Critical State Theory (*ACST* for short) proposed by Li and Dafalias (2012), which forms an extension of classical Critical State Theory (Schofield and Wroth, 1968). Theoretical aspects of ACST have been studied by Theocharis et al. (2017b, 2019), while experimental evidence for ACST from x-ray tomography measurements has been recently reported by Zhao et al. (2021). Furthermore, Hu et al. (2021) have recently explored implications of ACST for model parameters in a class of fabric evolution laws.

The stress–strain response of granular materials generally depends on loading direction, in particular for geomaterials subjected to complex loadings with changing direction, such as offshore geo-structures that are subjected to cyclic loads from wind and water waves. Such loads are then transferred to the supporting foundations, and hence the adjacent soils are sheared due to loadings with evolving directions. Therefore, the investigation of the *fabric response to different loading directions* is important for developing (advanced) constitutive models to simulate the behaviour of granular materials.

The importance of loading direction to the fabric response has been shown in previous studies (Yang et al., 2008; Karapiperis et al., 2020) on samples with initial, inherent anisotropy (due to the deposition process). Additionally, it has been shown that the fabric also changes when a granular material is subjected to purely elastic loadings (O'Sullivan and Cui, 2009; Agnolin and Roux, 2007; Pouragha et al., 2019; Karapiperis et al., 2020).

To systematically investigate the fabric response of granular materials for various loading directions, the probing technique proposed by Gudehus (1979) is employed here. This technique originally has been used to systematically explore the stress–strain response to various loading directions by studying the strain (or stress) response of the material to small imposed stress (or strain) increments along different loading paths. The stress probing technique, conveniently executed via two-dimensional DEM simulations, has been used in Pouragha et al. (2019, 2021) and Pouragha (2022) to study specific aspects of the fabric and strain response.

Pouragha et al. (2019) investigated the fabric response to strain probes where the initial samples are two-dimensional, isotropic samples. The fabric response to the strain probes has been determined via extensive sets of DEM simulations of the probes on samples of various initial void ratios. Although the stress response was 'pseudo-elastic' (with negligible plastic strains), the appreciable fabric response was shown to depend strongly on the strain probe direction (i.e. incrementally nonlinear behaviour is observed). Separate relationships have been formulated for the contributions due to the three mechanisms (i.e. contact disruption, creation and reorientation) of fabric evolution, that account for the difference in behaviour between compressive and tensile probes.

Moreover, a DEM simulation study of plastic flow of two-dimensional anisotropic samples has been performed by Pouragha et al. (2021). The considered samples have been obtained from a DEM simulation of monotonic biaxial isobaric compression, where periodic boundaries have been employed to suppress the formation of persistent, large-scale shear bands. For samples selected from the pre-peak loading part of the biaxial deformation simulation, extensive sets of DEM simulations of stress probes have been performed. Coaxial, 'in-plane' (inside the 'plane' in tensorial space that is spanned by the identity tensor and the current anisotropic stress/fabric tensor) as well as non-coaxial, 'out-of-plane' probes have been considered. Note that for the considered samples, the stress and fabric tensors are coaxial at the onset of probing. The in-plane plastic flow response corresponds to a classical flow rule, but the observed plastic flow in general is non-coaxial in the presence of out-of-plane stress components. It has been shown that the essential characteristics of the plastic flow are captured by a multi-mechanism plasticity theory.

Using the DEM data of probes of Pouragha et al. (2021), Pouragha (2022) has investigated the most important variables that drive fabric evolution by a systematic correlation analysis between increments of the fabric, stress, plastic and total strain tensors. Interestingly, it is found that the total strain rate is the best descriptor of the fabric rate, rather than the plastic strain rate that is used in many fabric evolution laws in literature. It should be mentioned that in this study the contact normal-based fabric tensor is considered.

The two-dimensional case has been considered in Pouragha et al. (2019, 2021) and Pouragha (2022). For three-dimensional cases, both the in-plane and the out-of-plane spaces occupy higher dimensions, and hence a more complex decomposition is required to generalise the non-coaxial formulation. This increases the complexity in the interpretation of results of DEM simulations. Although the numerical simulations here have been limited to two-dimensional cases, the basics of the formulation are developed in a general form that can serve as a starting point for further extensions to three-dimensional cases.

Here the fabric response to various loading directions is investigated in detail for a number of two-dimensional, *anisotropic* samples, using the results of DEM simulations from Pouragha et al. (2021). The current study extends that of Pouragha et al. (2019) on isotropic samples. The specific objectives are to:

- Analyse in detail (for the first time, to the best of the authors' knowledge) the fabric response of anisotropic samples to various loading directions through extensive sets of stress probes that include coaxial, in-plane probes as well as non-coaxial, out-of-plane probes (outside of the 'plane' corresponding to the current stress and fabric tensors).
- Develop a fabric evolution law (with a modest number of model parameters) that is adequate in describing, for all probes, the fabric response observed from the DEM simulations, for a number of anisotropic pre-peak samples with different values of stress ratio (and void ratio and fabric anisotropy). Note that the focus here is on investigating and describing the fabric response to all loading directions (for a number of samples), rather than on formulating a fabric evolution law that is valid throughout specific (monotonic) loading conditions.

Some notations used throughout this study are listed below. The rate of change with time of a second-order tensor $\boldsymbol{A}$ is denoted by $\dot{\boldsymbol{A}}$. The deviatoric part of a tensor $\boldsymbol{A}$ is denoted by $\boldsymbol{A}_{\text{dev}}$. The (unit) 'direction' tensor corresponding to $\boldsymbol{A}$ is denoted by $\hat{\boldsymbol{A}}$. These are defined by

$$\boldsymbol{A}_{\text{dev}} = \boldsymbol{A} - \frac{1}{2}\text{tr}(\boldsymbol{A})\boldsymbol{I} \qquad \hat{\boldsymbol{A}} = \frac{\boldsymbol{A}}{\|\boldsymbol{A}\|}, \tag{1}$$

where $\boldsymbol{I}$ is the second-order identity tensor, the trace of $\boldsymbol{A}$ is given by $\text{tr}(\boldsymbol{A}) = \boldsymbol{A} : \boldsymbol{I}$ and $\|\boldsymbol{A}\| = \sqrt{\boldsymbol{A} : \boldsymbol{A}}$ is the Euclidean norm of $\boldsymbol{A}$.

The employed sign convention for stress $\boldsymbol{\sigma}$ and strain $\boldsymbol{\epsilon}$ is that compressive stresses and strains are considered to be positive. In the two-dimensional case considered here, the mean pressure p, the deviatoric stress tensor $\boldsymbol{\tau}$ and the (scalar) stress deviator q are defined by

$$p = \frac{1}{2}\text{tr}(\boldsymbol{\sigma}) \qquad \boldsymbol{\tau} = \boldsymbol{\sigma} - p\boldsymbol{I} \qquad q = \sqrt{\frac{1}{2}\boldsymbol{\tau} : \boldsymbol{\tau}}. \tag{2}$$

The unit direction tensors, defined by Eq. (1), corresponding to $\boldsymbol{I}$ and $\boldsymbol{\tau}$ are $\hat{\boldsymbol{I}}$ and $\hat{\boldsymbol{\tau}}$, respectively.

The overview of this study is as follows. In Section 2 the fabric tensor is defined. The DEM simulations of the probes from Pouragha et al. (2021), whose results are analysed here, are briefly described in Section 3. The main results for the fabric response to the probes are presented in Section 4. A theoretical description of these results is given in Section 5. Finally, findings of this study are discussed in Section 6.

2. Fabric tensor

In the absence of long-range forces, the particles in a granular sample only interact at interparticle contact points. For two particles p and q in contact, the branch vector $\boldsymbol{l}^{pq}$ is the vector connecting the centres of the two particles involved, i.e. $\boldsymbol{l}^{pq} = \boldsymbol{X}^q - \boldsymbol{X}^p$ where $\boldsymbol{X}^p$ and $\boldsymbol{X}^q$ are the global position vectors of the centres of particles p and q, respectively. The corresponding unit normal vector is denoted by $\boldsymbol{n}^{pq}$. Coordination number Z is the average number of contacts per particle, defined by

$$Z = 2N_c/N_p\,, \tag{3}$$

where N_p and N_c are, respectively, the number of particles and the number of contacts in the granular sample. In the determination of the coordination number, "rattlers" (i.e. particles that do not directly contribute to the mechanical stability of the system) have been disregarded, using the expression in Thornton (2000). Coordination number Z and void ratio e both describe the packing density of a sample.

The contact normal-based fabric tensor (Oda, 1972; Satake, 1978; Oda, 1982) that is studied here represents a statistical average of the orientation of the contact unit normal vectors $\boldsymbol{n}^c$. The symmetric, second-order fabric tensor $\boldsymbol{F}$ is defined by

$$F_{ij} = \frac{2}{N_p}\sum_{c\in C} n_i^c n_j^c\,, \tag{4}$$

where the summation is over contacts c in the set of contacts C in the region under consideration, and $\boldsymbol{n}^c$ is the unit contact normal associated with contact c; thus $n_i^c n_i^c = 1$. This definition for the fabric tensor, through the choice of scaling factor being N_p rather than N_c, also provides information on coordination number Z, since $\mathrm{tr}(\boldsymbol{F}) = Z$ (as follows from Eqs. (3) and (4); note that $\boldsymbol{n}^c$ is a unit vector).

The full fabric tensor $\boldsymbol{F}$, rather than only the deviatoric part $\boldsymbol{F}_{\mathrm{dev}}$, is considered here, since it contains additional relevant information on coordination number Z and in the two-dimensional case the deviatoric components of the fabric tensor in the (F_{11}, F_{22}) plane lie on a line with a slope of $\tan(-45°)$ through the origin (since $\mathrm{tr}(\boldsymbol{F}_{\mathrm{dev}}) = 0$ and hence $\mathrm{tr}(\dot{\boldsymbol{F}}_{\mathrm{dev}}) = 0$), and are therefore rather restricted, for in-plane probes.

In terms of the principal values F_1 and F_2 of the fabric tensor $\boldsymbol{F}$, coordination number Z and fabric anisotropy A are expressed by

$$Z = F_1 + F_2 \qquad A = F_1 - F_2\,. \tag{5}$$

For two-dimensional anisotropic samples, the stress tensor (coaxial with the fabric tensor for the samples considered here) lies in a 'plane' that is spanned by the tensors $\boldsymbol{I}$ and $\boldsymbol{\tau}$. A symmetric, second-order tensor $\boldsymbol{A}$ is decomposed into 'in-plane' and 'out-of-plane' parts (Pouragha et al., 2021), $\boldsymbol{A}^\pi$ and $\boldsymbol{A}^\rho$ respectively, by

$$\boldsymbol{A}^\pi = \mathrm{tr}(\boldsymbol{A}\cdot\hat{\boldsymbol{I}})\hat{\boldsymbol{I}} + \mathrm{tr}(\boldsymbol{A}\cdot\hat{\boldsymbol{\tau}})\hat{\boldsymbol{\tau}} \qquad \boldsymbol{A}^\rho = \boldsymbol{A} - \boldsymbol{A}^\pi\,. \tag{6}$$

The in-plane part $\boldsymbol{A}^\pi$ is coaxial with the current stress/fabric tensor, while the out-of-plane part $\boldsymbol{A}^\rho$ is non-coaxial. This decomposition will be primarily used here for the fabric rate $\dot{\boldsymbol{F}}$ and the strain rate $\dot{\boldsymbol{\epsilon}}$ tensors. A similar decomposition has been adopted in the framework of tangential plasticity (Rudnicki and Rice, 1975). For the considered two-dimensional samples, the (deviatoric) stress and fabric tensors are coaxial, and hence $\hat{\boldsymbol{\tau}} = \widehat{\boldsymbol{F}_{\mathrm{dev}}}$.

Note that the set consisting of identity tensor $\boldsymbol{I}$, deviatoric stress tensor $\boldsymbol{\tau}$ and out-of-plane strain rate $\dot{\boldsymbol{\epsilon}}^\rho$, $\{\boldsymbol{I}, \boldsymbol{\tau}, \dot{\boldsymbol{\epsilon}}^\rho\}$, forms an orthogonal basis for the space of symmetric second-order tensors in the two-dimensional case with anisotropic stress/fabric. For three-dimensional cases, a more complex decomposition is required to generalise the non-coaxial formulation, since both the in-plane and the out-of-plane spaces occupy higher dimensions.

A simple model for fabric evolution that is based on the uniform-strain assumption is given in Appendix A, showing that the variable $\boldsymbol{F}\cdot\dot{\boldsymbol{\epsilon}}$ is important for fabric evolution.

Table 1
Properties of the samples subjected to stress probes: coordination number Z, fabric anisotropy A and void ratio e, for various stress ratios q/p. The mean pressure p is the same for all samples, with $p/(E\bar{r}) = 5\times10^{-3}$.

q/p	Z	A	e
0.15	4.302	0.049	0.1974
0.30	4.159	0.135	0.1976
0.40	3.997	0.233	0.1982
0.44	3.846	0.320	0.1984

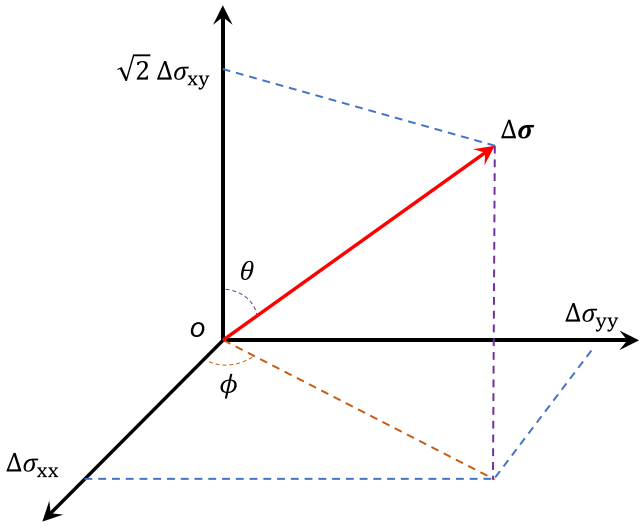

Fig. 1. Components of the increment of the stress tensor, $\Delta\boldsymbol{\sigma}$, for a stress probe that is characterised by the polar angles ϕ and θ.

3. DEM simulations of stress probes

The study in Pouragha et al. (2019) explored the fabric response of two-dimensional *isotropic* granular samples, through strain probes without shear strains. In the current study, the samples were loaded deviatorically to desired stress states, and hence the state of the material at the onset of probing is anisotropic. The stress probes that have been applied to these anisotropic samples involve shear components. Hence, non-coaxial probes have also been considered that lie outside of the stress/fabric plane.

The details of DEM simulations that are analysed here have been described in Pouragha et al. (2021). The main points of the numerical simulations are briefly described here for completeness.

The numerical simulations were performed using the open-source code YADE (Smilauer et al., 2015). Samples with 50,000 circular particles, with radii uniformly distributed between r_{min} and r_{max} where $r_{max}/r_{min} = 2$, were initially generated.

The elastic part of the interparticle contact model involves linear springs in the directions normal and tangential to the contact, with equal stiffnesses k^c. The contact stiffnesses have been determined from $k^c = E\frac{2r_1^c r_2^c}{r_1^c + r_2^c}$, where E is an elastic modulus and r_1^c and r_2^c are the radii of the particles involved in contact c. For the frictional part, a cohesionless Coulomb model with interparticle friction angle of 30° has been used.

The initial sample was isotropically compressed to the desired confining mean pressure p_0, with periodic boundaries being employed to reduce spatial heterogeneities induced by physical walls. Parameters E and p_0 have been selected such that the contact deformation is small relative to the average particle radius; $p_0/(E\bar{r}) = 5\times10^{-3}$ where $\bar{r}$ is the average particle radius. The (two-dimensional) void ratio of the resulting dense sample equals 0.1958.

The initial sample was subsequently sheared, while keeping the mean pressure p constant (i.e. $p = p_0$), to the stress ratio q/p of 0.15,

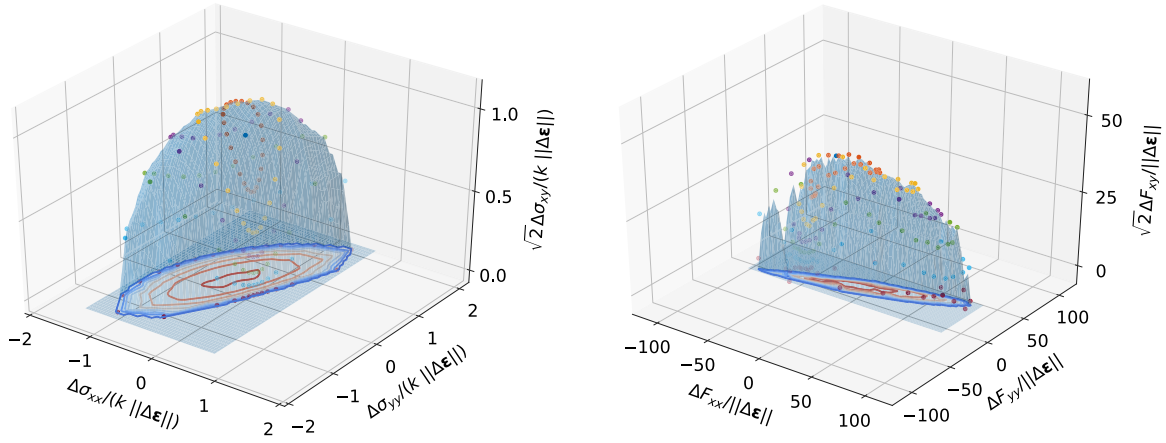

Fig. 2. Response to strain probes: (left) stress response $\Delta\boldsymbol{\sigma}$, scaled with contact stiffness k and magnitude of the strain increment, $\|\Delta\boldsymbol{\epsilon}\|$; (right) fabric response $\Delta\boldsymbol{F}$, scaled with magnitude of the strain increment, $\|\Delta\boldsymbol{\epsilon}\|$. Results for the system with $q/p = 0.40$. The x and y directions correspond to the minor and major principal stress/fabric directions, respectively.

0.30, 0.40 and 0.44 (the peak stress ratio is 0.48). The evolution of stress ratio and of volumetric strain with respect to deviatoric strain are shown in Fig. 1 of Pouragha et al. (2021) and Pouragha (2022). Information on the samples (coordination number Z, fabric anisotropy A and void ratio e) for these stress ratios is given in Table 1. A Cartesian coordinate system (x, y) is employed in the following such that the x and y directions correspond to the minor and major principal stress/fabric directions, respectively.

Starting from these stored samples, stress probes were performed using servo-control techniques. For each probe, the norm of the stress increment $\|\Delta\boldsymbol{\sigma}\|$ was the same. For a given probe, the components of the stress increment tensor $\Delta\boldsymbol{\sigma}$ are given by (see also Fig. 1):

$$\begin{bmatrix} \Delta\sigma_{xx} & \Delta\sigma_{xy} \\ \Delta\sigma_{yx} & \Delta\sigma_{yy} \end{bmatrix} = \|\Delta\boldsymbol{\sigma}\| \begin{bmatrix} \sin\theta\cdot\cos\phi & \frac{1}{\sqrt{2}}\cos\theta \\ \frac{1}{\sqrt{2}}\cos\theta & \sin\theta\cdot\sin\phi \end{bmatrix}, \tag{7}$$

where θ varies from 0° to 90° with an increment of 15° (7 values); ϕ varies from 0° to 360° with an increment of 15° (25 values, but it should be noted that $\phi = 0°$ is equivalent to $\phi = 360°$). These stress probes can be categorised into two types (Pouragha et al., 2019):

- in-plane probes: $\theta = 90°$; hence $\Delta\sigma_{xy} = 0$
- out-of-plane probes: $\theta \in [0, 90°)$; hence $\Delta\sigma_{xy} \neq 0$

The size of the stress probes, $\|\Delta\boldsymbol{\sigma}\|$, is dictated by the requirement that the response variables remain homogeneous of degree one with respect to the probe size (Froiio and Roux, 2010; Pouragha et al., 2019). This leads to an upper bound for the probe size, which decreases as the plastic mechanisms become more prevalent closer to the stress peak. Moreover, for the study of fabric evolution, a practical lower bound also exists for the probe size to ensure statistically representative changes in fabric. Using trial-and-error approach, a probe size of $\|\Delta\boldsymbol{\sigma}\| = 0.01\, p_0$ has been adopted in this study. Upon detailed examination (data not shown), the strain and fabric responses are found to be linear with an adequate level of accuracy.

4. Fabric response to probes

Since the DEM probes in Pouragha et al. (2021) are based on stress probes with identical magnitude $\|\Delta\boldsymbol{\sigma}\|$ of the stress increment tensor $\Delta\boldsymbol{\sigma}$ and the analyses by Pouragha (2022) have shown that the main variable driving fabric evolution is the strain rate tensor $\dot{\boldsymbol{\epsilon}}$ (also confirmed theoretically by the uniform-strain theory in Appendix A and the graphical representation of the DEM results in Appendix B), the probe responses, in terms of stress increment $\Delta\boldsymbol{\sigma}$ and fabric increment $\Delta\boldsymbol{F}$, have been 'converted' to strain probes by scaling (for each probe separately) with the magnitude of the strain increment $\|\Delta\boldsymbol{\epsilon}\|$. Therefore, the (thus converted) strain increments of the probes lie on a unit sphere in strain-increment space.

The corresponding responses, in terms of the scaled stress increments $\Delta\boldsymbol{\sigma}/\|\Delta\boldsymbol{\epsilon}\|$ and the scaled fabric increments $\Delta\boldsymbol{F}/\|\Delta\boldsymbol{\epsilon}\|$, are shown in Fig. 2. The relation between (plastic) strain increments and stress increments has been analysed in detail in Pouragha et al. (2021); the focus here is on the fabric response. Qualitatively, the shape of the fabric response resembles an ellipsoid (with large aspect ratios). This indicates a *linear* mapping between the strain rate $\dot{\boldsymbol{\epsilon}}$ and the fabric rate $\dot{\boldsymbol{F}}$, as is shown in more detail in Section 5. The fabric rate $\dot{\boldsymbol{F}}$ is *non-linear* in the stress rate $\dot{\boldsymbol{\sigma}}$ due to the non-linear (elasto-plastic) relation (bilinear in character) between stress rate and strain rate (Pouragha et al., 2021).

Here a brief analysis of correlation between in-plane and out-of-plane components of fabric increments and (total) strain increments has been performed. The analysis of the correlation coefficient between the in-plane part of the fabric increment $\Delta\boldsymbol{F}^{\pi}$ and the out-of-plane strain increment $\Delta\boldsymbol{\epsilon}^{\rho}$ and between the out-of-plane part of the fabric increment $\Delta\boldsymbol{F}^{\rho}$ and the in-plane strain increment $\Delta\boldsymbol{\epsilon}^{\pi}$ showed that these cross-couplings are fairly small. The correlation coefficient between the scaled in-plane fabric increment $\Delta\boldsymbol{F}^{\pi}/\|\Delta\boldsymbol{\epsilon}\|$ and the scaled out-of-plane strain increment $\Delta\boldsymbol{\epsilon}^{\rho}/\|\Delta\boldsymbol{\epsilon}\|$ is found to be about 0.11; the correlation coefficient between the scaled out-of-plane fabric increment $\Delta\boldsymbol{F}^{\rho}/\|\Delta\boldsymbol{\epsilon}\|$ and the scaled in-plane strain increment $\Delta\boldsymbol{\epsilon}^{\pi}/\|\Delta\boldsymbol{\epsilon}\|$ is about 0.17. These values have been averaged over the considered samples.

Considering these weak correlations, the in-plane fabric increment is considered to be independent of the out-of-plane strain increment and the out-of-plane fabric increment is considered to be independent of the in-plane strain increment. Hence it is assumed here that the two parts of the fabric increment only depend on the corresponding strain increment: $\Delta\boldsymbol{F}^{\pi} = \boldsymbol{G}^{\pi}(\Delta\boldsymbol{\epsilon}^{\pi})$ and $\Delta\boldsymbol{F}^{\rho} = \boldsymbol{G}^{\rho}(\Delta\boldsymbol{\epsilon}^{\rho})$. This suggests that the in-plane and out-of-plane fabric responses are decoupled. In contrast, the results in Pouragha et al. (2021) show that such a decoupling assumption does not apply to the stress–strain response where in-plane plastic strains are observed as a result of out-of-plane stress increments.

Firstly the results for $q/p = 0.40$ of the *in-plane* probes are shown in Fig. 3; for other samples corresponding to different values of stress ratio q/p qualitatively similar results are obtained. These results for the fabric response for the in-plane probes resemble an elliptical shape. A detailed description is given in Section 5.

The relation between the out-of-plane fabric increment $\Delta\boldsymbol{F}^{\rho}$ and the out-of-plane strain increment $\Delta\boldsymbol{\epsilon}^{\rho}$ is shown in Fig. 4, which shows that $\Delta\boldsymbol{F}^{\rho}$ is proportional to $\Delta\boldsymbol{\epsilon}^{\rho}$, with acceptable accuracy. Minor out-of-plane increments of fabric are also observed for the in-plane probes. However, these increments are of the same order of magnitude as the scatter in the rest of the data, and are therefore not considered to be of mechanical importance.

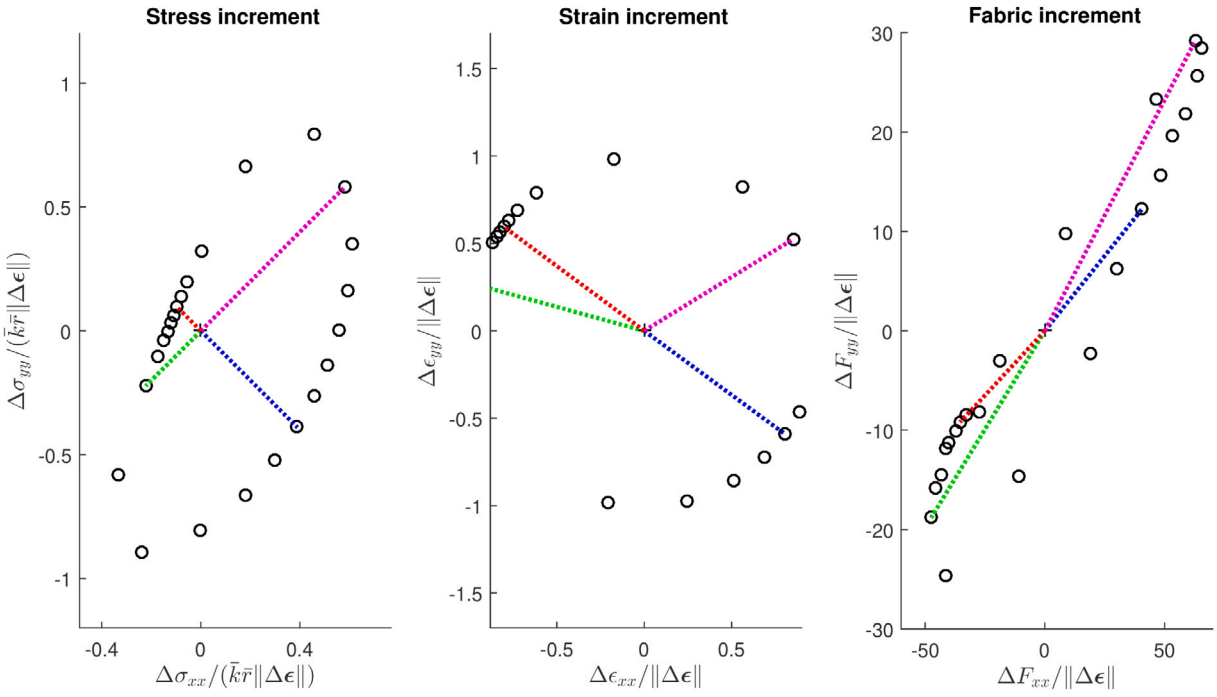

Fig. 3. Results of the in-plane stress probes for $q/p = 0.40$. Left: Imposed stress increment, scaled with the magnitude of the corresponding (total) strain increment, average contact stiffness $\bar{k}$ and particle radius $\bar{r}$. Middle: Scaled strain increment (and hence corresponding to the unit circle). Right: Fabric increment, scaled with the magnitude of the corresponding (total) strain increment. To aid in the interpretation, some characteristic probes (with 'directions' $\phi = -135°$ (in green), $\phi = -45°$ in (blue) $\phi = +45°$ (in magenta) and $\phi = +135°$ (in red); ϕ is defined in Fig. 1) are indicated by dotted lines in all subfigures. The subfigures on the left and in the middle have equal horizontal and vertical scales. The x and y directions correspond to the minor and major principal stress/fabric directions, respectively.

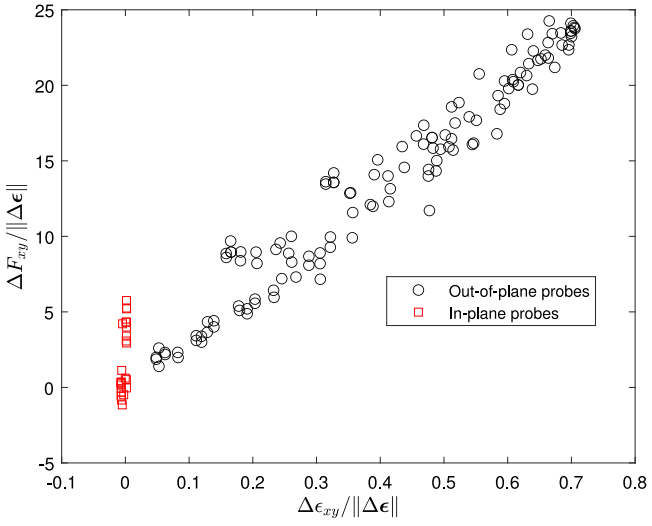

Fig. 4. Dependence of the scaled out-of-plane fabric increment $\Delta\boldsymbol{F}^{\rho}$ (component ΔF_{xy}) on the scaled out-of-plane strain increment $\Delta\boldsymbol{\epsilon}^{\rho}$ (component $\Delta\epsilon_{xy}$, with the employed coordinate system).

5. Theoretical description

Inspired by the observations of the results of the DEM simulations shown in Section 4, the objective of this Section is to develop an expression for the fabric rate $\dot{\boldsymbol{F}}$ in terms of the strain rate $\dot{\boldsymbol{\epsilon}}$ that is reasonably accurate for all, in-plane as well as out-of-plane, probes. The fabric rate may depend on various characteristics, such as the stress rate $\dot{\boldsymbol{\sigma}}$, the (total) strain rate $\dot{\boldsymbol{\epsilon}}$ and/or the plastic strain rate $\dot{\boldsymbol{\epsilon}}^{p}$. An overview of different classes of fabric evolution models has been given by Zhao and Kruyt (2020).

The analyses by Pouragha (2022) have shown that the fabric rate $\dot{\boldsymbol{F}}$ is predominantly driven by the total strain rate $\dot{\boldsymbol{\epsilon}}$, and hence the following general expression for the fabric rate is investigated

$$\dot{\boldsymbol{F}} = \boldsymbol{G}(\dot{\boldsymbol{\epsilon}}; \boldsymbol{S}) . \tag{8}$$

Here, $\boldsymbol{S}$ is some 'state' vector set, which consists of current stress tensor $\boldsymbol{\sigma}$, current fabric tensor $\boldsymbol{F}$ and/or void ratio (or a combination of these, such as the stress ratio q/p and the state parameter $\psi = e - e_c(p)$ (Been and Jefferies, 1985) used in the fabric evolution law in Zhao and Kruyt (2020), where e_c is the void ratio at the critical state). Since quasi-static, rate-independent behaviour of granular materials is considered, Eq. (8) must be positively homogeneous of degree one in $\dot{\boldsymbol{\epsilon}}$.

When analysing a set of probes from a specific sample at a given stress condition, the state vector set $\boldsymbol{S}$ is the same for all probes. Therefore, for convenience in notation, the dependence on $\boldsymbol{S}$ in Eq. (8) is dropped in the following, and hence it will be expressed as $\dot{\boldsymbol{F}} = \boldsymbol{G}(\dot{\boldsymbol{\epsilon}})$, with the understanding that all model parameters may depend on $\boldsymbol{S}$ (as well as on DEM material properties, such as friction angles).

Since the in-plane fabric response is independent of the out-of-plane strain increment and the out-of-plane fabric response is independent of the in-plane strain increment (see Section 4), $\dot{\boldsymbol{F}}^{\pi} = \boldsymbol{G}(\dot{\boldsymbol{\epsilon}}^{\pi})$ and $\dot{\boldsymbol{F}}^{\rho} = \boldsymbol{G}(\dot{\boldsymbol{\epsilon}}^{\rho})$. For the out-of-plane part of the fabric increment, the results shown in Fig. 4 indicate that the out-of-plane fabric increment is proportional to the out-of-plane strain increment

$$\dot{\boldsymbol{F}}^{\rho} = d_{\rho}\dot{\boldsymbol{\epsilon}}^{\rho} , \tag{9}$$

where d_{ρ} is the proportionality factor. Compared to the out-of-plane fabric response, the in-plane fabric response $\dot{\boldsymbol{F}}^{\pi}$ is more complicated. This response is analysed in the following subsection.

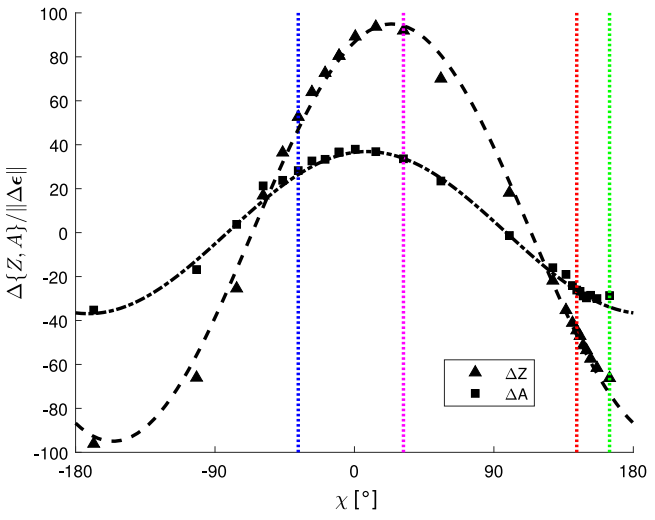

Fig. 5. Scaled increment in coordination number ΔZ and fabric anisotropy ΔA for the in-plane probes. Shown are DEM results for the probes (markers) for the sample with $q/p = 0.40$, and fits (dashed curves) according to Eq. (12). The vertical lines indicate some characteristic probes, with 'directions' $\phi = -135°$ (in green), $\phi = -45°$ in (blue), $\phi = +45°$ (in magenta) and $\phi = +135°$ (in red); ϕ and χ are defined through Eq. (11).

5.1. In-plane fabric response

The correlation analysis in Section 4 showed that the in-plane fabric increment is effectively only dependent on the in-plane strain increment. The results in Fig. 3 for the fabric response for the in-plane probes resemble an elliptical shape (with a large aspect ratio). This can be described by a linear relationship

$$\dot{\boldsymbol{F}}^{\pi} = \boldsymbol{H}^{\pi\pi} : \dot{\boldsymbol{\epsilon}}^{\pi}\,, \tag{10}$$

since such a linear mapping transforms a circle in the in-plane strain increment space (corresponding to probes with identical $\|\Delta\boldsymbol{\epsilon}\|$) to an ellipse in the in-plane fabric increment space; here $\boldsymbol{H}^{\pi\pi}$ is a fourth-order tensor.

For *in-plane* probes, the normalised stress rate tensor $\hat{\dot{\boldsymbol{\sigma}}}$ and the normalised strain rate tensor $\hat{\dot{\boldsymbol{\epsilon}}}$ can be written as

$$\hat{\dot{\boldsymbol{\sigma}}} = \begin{pmatrix} \cos\phi & 0 \\ 0 & \sin\phi \end{pmatrix} \qquad \hat{\dot{\boldsymbol{\epsilon}}} = \begin{pmatrix} \cos\chi & 0 \\ 0 & \sin\chi \end{pmatrix}. \tag{11}$$

The former follows from Eq. (7) (see also Fig. 1, with $\theta = 90°$); the normalisation is defined in Eq. (1). In general, with the stress increment $\Delta\boldsymbol{\sigma}$ (with corresponding ϕ) prescribed in the current stress probes, the strain increment $\Delta\boldsymbol{\epsilon}$ (with corresponding χ measured relative to the $\Delta\epsilon_{xx}$ direction) is a *response*; hence $\chi = \chi(\phi)$. In the following some characteristic in-plane probe 'directions' are indicated, with $\phi = -135°, -45°, +45°, +135°$. The direction of continued loading in the isobaric test from which the initial samples for the probes (with different values of the stress ratio q/p) have been obtained corresponds to $\phi = +135°$, while reversed loading corresponds to $\phi = -45°$.

The results for the in-plane fabric response, $\dot{F}_{xx}$ and $\dot{F}_{yy}$ for the employed coordinate system, are equivalently but more conveniently analysed in terms of the rate of coordination number $\dot{Z}$ and the rate of fabric anisotropy $\dot{A}$. These are analysed for the in-plane probes as function of 'direction' χ (defined in Eq. (11)). The scaled increments of the coordination number and the fabric anisotropy, $\Delta Z/\|\Delta\boldsymbol{\epsilon}\|$ and $\Delta A/\|\Delta\boldsymbol{\epsilon}\|$ respectively, are shown in Fig. 5 (for $q/p = 0.40$). The results show that $\dot{Z}$ and $\dot{A}$ from the DEM simulations of the in-plane probes can well be described by

$$\dot{Z} = a_Z \cos\chi + b_Z \sin\chi \qquad \dot{A} = a_A \cos\chi + b_A \sin\chi\,, \tag{12}$$

where a_Z, b_Z, a_A and b_A are model parameters.

The maximum in the rate of coordination number $\dot{Z}$ for the in-plane probes is attained at a direction $\chi_{\max}$. Fig. 5 indicates that this direction is different from $\phi = 45°$ (that corresponds to an isotropic compressive stress increment in the probe) and from $\chi = 45°$ (that corresponds to an isotropic compressive strain increment in the probe); $\chi_{\max}$ varies from 13° for $q/p = 0.15$ to 35° for $q/p = 0.44$.

The results in Fig. 5 show that $\dot{A}$ is nearly symmetrical around $\chi = 0$, which implies that b_A in Eq. (12) is fairly small, $b_A \approx 0$ ($b_A/a_A = 0.004$ for $q/p = 0.15$; $b_A/a_A = 0.28$ for $q/p = 0.44$).

The expressions in Eq. (12) (involving four parameters) for the rates of coordination number $\dot{Z}$ and fabric anisotropy $\dot{A}$ determine the fourth-order tensor $\boldsymbol{H}^{\pi\pi}$ (also involving four parameters) in Eq. (10) that relates the in-plane strain rate $\dot{\boldsymbol{\epsilon}}^{\pi}$ to the in-plane fabric rate $\dot{\boldsymbol{F}}^{\pi}$. A relationship of the type Eq. (10), and involving four model parameters d_1, d_2, d_3, d_4, is retrieved in tensorial form by

$$\dot{\boldsymbol{F}}^{\pi} = \left[d_1 \mathrm{tr}(\dot{\boldsymbol{\epsilon}}) + d_2 \mathrm{tr}(\dot{\boldsymbol{\epsilon}}^{\pi}_{\mathrm{dev}} \cdot \hat{\boldsymbol{\tau}})\right] \hat{\boldsymbol{I}} + \left[d_3 \mathrm{tr}(\dot{\boldsymbol{\epsilon}}) + d_4 \mathrm{tr}(\dot{\boldsymbol{\epsilon}}^{\pi}_{\mathrm{dev}} \cdot \hat{\boldsymbol{\tau}})\right] \hat{\boldsymbol{\tau}}\,. \tag{13}$$

This expression is based on: (i) the in-plane space of symmetric second-order tensors being spanned by $\{\boldsymbol{I}, \boldsymbol{\tau}\}$ and (ii) that for objectivity and linearity in the in-plane strain rate $\dot{\boldsymbol{\epsilon}}^{\pi}$, the in-plane fabric rate $\dot{\boldsymbol{F}}^{\pi}$ must depend linearly on the strain rate invariant $\mathrm{tr}(\dot{\boldsymbol{\epsilon}})$ and the joint invariant $\mathrm{tr}(\dot{\boldsymbol{\epsilon}}^{\pi}_{\mathrm{dev}} \cdot \hat{\boldsymbol{\tau}})$ of the deviatoric strain rate and the (scaled) stress tensor. Note that $\mathrm{tr}(\dot{\boldsymbol{\epsilon}}) = \mathrm{tr}(\dot{\boldsymbol{\epsilon}}^{\pi})$ and that the term $\mathrm{tr}(\dot{\boldsymbol{\epsilon}}^{\pi}_{\mathrm{dev}} \cdot \hat{\boldsymbol{\tau}})$ can be expressed as $\frac{1}{\sqrt{2}}\left(\dot{\epsilon}^{\pi}_1 - \dot{\epsilon}^{\pi}_2\right)$, where $\dot{\epsilon}^{\pi}_1$ and $\dot{\epsilon}^{\pi}_2$ are the principal values of the in-plane strain rate tensor $\dot{\boldsymbol{\epsilon}}^{\pi}$.

Using Eqs. (5) and (11), it follows from Eq. (13) that for in-plane probes the rate of coordination number $\dot{Z}$ and of fabric anisotropy $\dot{A}$ are given by

$$\begin{aligned} \dot{Z} &= (+\sqrt{2}d_1 - d_2)\cos\chi + (\sqrt{2}d_1 + d_2)\sin\chi \\ \dot{A} &= (-\sqrt{2}d_3 + d_4)\cos\chi - (\sqrt{2}d_3 + d_4)\sin\chi\,. \end{aligned} \tag{14}$$

Consequently, it follows from Eqs. (12) and (14) that the relation $b_A \approx 0$ is equivalent to $d_4 \approx -\sqrt{2}d_3$.

5.2. Full fabric evolution law and model parameters

The results in Section 4 have shown that the in-plane and out-of-plane responses are effectively decoupled. Therefore, the complete fabric evolution law is obtained by combining Eqs. (9) and (13) for the out-of-plane and the in-plane fabric response, respectively

$$\dot{\boldsymbol{F}} = \left[d_1 \mathrm{tr}(\dot{\boldsymbol{\epsilon}}) + d_2 \mathrm{tr}(\dot{\boldsymbol{\epsilon}}^{\pi}_{\mathrm{dev}} \cdot \hat{\boldsymbol{\tau}})\right] \hat{\boldsymbol{I}} + \left[d_3 \mathrm{tr}(\dot{\boldsymbol{\epsilon}}) + d_4 \mathrm{tr}(\dot{\boldsymbol{\epsilon}}^{\pi}_{\mathrm{dev}} \cdot \hat{\boldsymbol{\tau}})\right] \hat{\boldsymbol{\tau}} + d_\rho \dot{\boldsymbol{\epsilon}}^{\rho}\,. \tag{15}$$

Model parameters d_1 and d_2 determine the rate of coordination number $\dot{Z}$. Parameter d_1 is the proportionality factor between the rate of coordination number $\dot{Z}$ and the volumetric strain rate $\mathrm{tr}(\dot{\boldsymbol{\epsilon}})$. Compression leads to an increase of coordination number, so $d_1 > 0$. Parameters d_3 and d_4 determine the rate of fabric anisotropy $\dot{A}$. Parameter d_ρ is the proportionality factor between the out-of-plane fabric rate $\dot{\boldsymbol{F}}^{\rho}$ and the out-of-plane strain rate $\dot{\boldsymbol{\epsilon}}^{\rho}$.

The accuracy of the model description Eq. (15) is assessed in Fig. 6 by comparing the fabric increments from the DEM simulations of the probes with the corresponding fabric increments according to the model (Eq. (15)). Fig. 6 shows the good agreement between the results of the DEM simulations of the (large number of) probes and the theoretical description Eq. (15), with model parameters determined by a least-squares method.

The model parameters d_1, d_2, d_3, d_4 and d_ρ in Eq. (15) for the fabric rate may depend on the state vector set $\boldsymbol{S}$ (involving current stress, fabric, void ratio). The model parameters have been determined for the samples corresponding to $q/p = 0.15$, $q/p = 0.30$, $q/p = 0.40$ and $q/p = 0.44$. The resulting parameters are shown in Fig. 7 as function of fabric anisotropy A (rather than q/p), since it shows a linear relationship for the parameters d_2 and d_4. These values with corresponding stress ratios are also reported in Table 2 in Appendix C. Parameters d_1, d_2, d_3, d_4

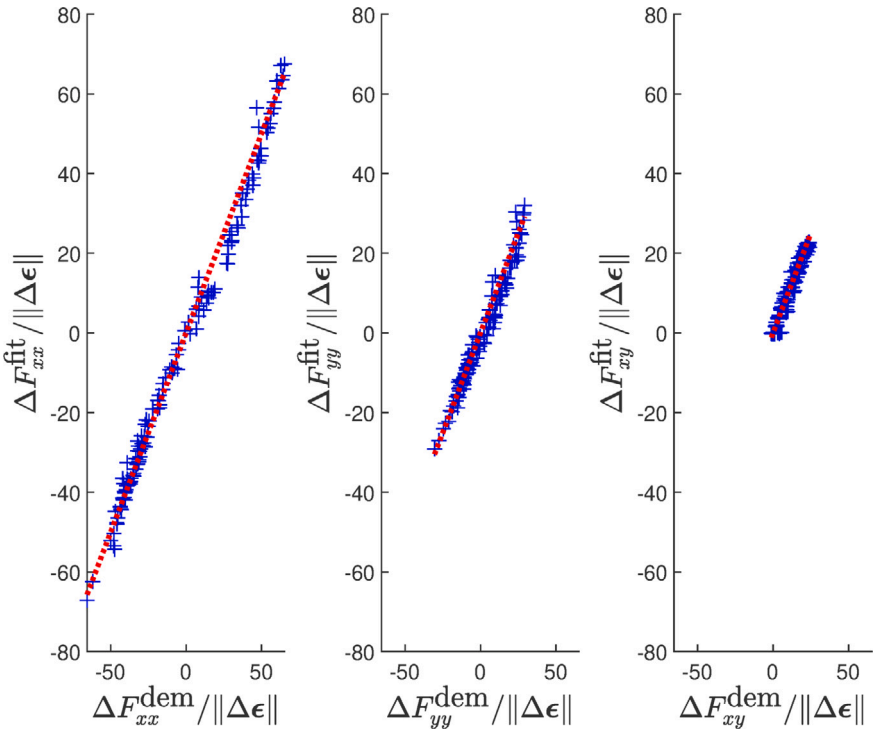

Fig. 6. Comparison between the components of the scaled fabric increments $\Delta\boldsymbol{F}/\|\Delta\boldsymbol{\epsilon}\|$ from the DEM simulations of the probes and those according to Eq. (15), with fitted model parameters; $1-R^2=0.0056$; results for the sample with $q/p=0.40$. The red dashed line at 45° through the origin has been added to facilitate the comparison; a perfect fit of the data corresponds to this line. The x and y directions correspond to the minor and major principal stress/fabric directions, respectively.

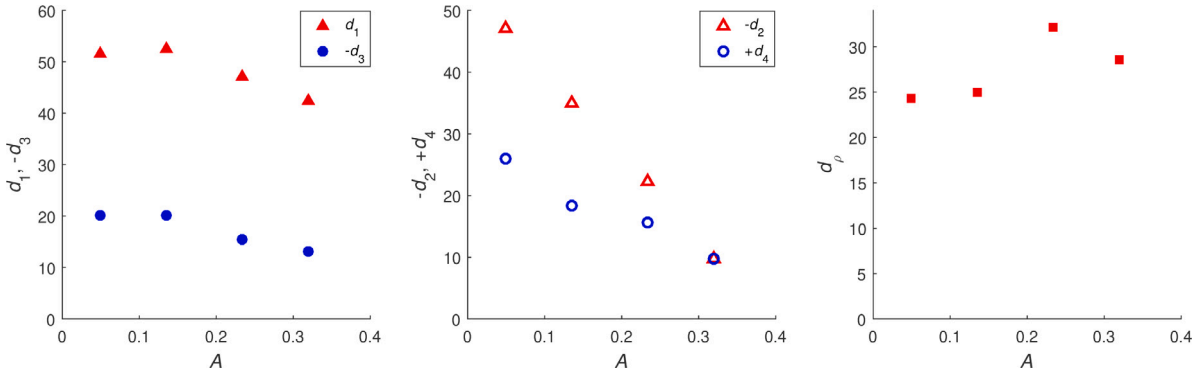

Fig. 7. Variation of model parameters d_1, d_2, d_3, d_4, d_ρ in Eq. (15) with fabric anisotropy A. Values for these parameters are given in Table 2 in Appendix C.

involved in the in-plane fabric response decrease (in absolute values) with increasing fabric anisotropy A; the variations of d_1, d_3 and d_ρ with A are fairly modest. The approximate relation for d_4, $d_4 \approx -\sqrt{2}d_3$, fairly accurately corresponds to the fitted results, especially for the system with small values of q/p (as can be verified with the values given in Table 2).

The values for the model parameters d_1, d_2, d_3, d_4 and d_ρ reported in Table 2 have been determined for a number of samples with different values of the stress ratio q/p and identical mean pressure p. To generalise the developed evolution law so that it can be used in (advanced) constitutive modelling of granular soils, these parameters should be given as functions of the state vector set $\boldsymbol{S}$ (see Eq. (8), involving in particular stress ratio q/p, void ratio e, mean pressure p (or combined via the state function $\psi = e - e_c(p)$ (Been and Jefferies, 1985) as in Zhao and Kruyt, 2020)). In particular, parameters d_1 and d_2 that affect the rate of coordination number are expected to depend on the mean pressure p. However, the current data (based on four samples with the same mean pressure p) is not sufficient to formulate closed-form expressions for these parameters.

5.3. Consistency with ACST and potential simplifications

In this subsection some aspects of the fabric evolution law, Eq. (15), are discussed: (i) consistency with ACST and (ii) possibilities for further simplification.

According to ACST, at large strains, continued deformation occurs with constant volume, $\mathrm{tr}(\dot{\boldsymbol{\epsilon}})=0$, as well as constant fabric, $\dot{\boldsymbol{F}}=\boldsymbol{0}$. The ACST condition $\dot{\boldsymbol{F}}=\boldsymbol{0}$ is met when $d_2=0$ and $d_4=0$ at the critical state. There are no requirements for model parameters d_1 and d_3, since $\mathrm{tr}(\dot{\boldsymbol{\epsilon}})=0$ at the critical state. Note that d_ρ does not need to be equal to zero at the critical state, since a change of loading direction that is out-of-plane may still lead to changes in the fabric tensor. The results for d_2 and d_4 shown in Fig. 7 show a decrease of these parameters with increasing q/p, consistent with the ACST requirement as the critical state is approached. However, the current data (limited to samples with pre-peak values for q/p) is not sufficient to confirm that these conditions indeed hold at the critical state.

The analysis in Section 5.1 showed that approximately $b_A=0$, which is equivalent to $d_4=-\sqrt{2}d_3$. When this relation is employed, the

number of model parameters is reduced to four (d_1, d_2, d_3 and d_ρ). The in-plane fabric response is elliptical in shape, see Fig. 3, with a large aspect ratio. A response that lies on a line (corresponding to an aspect ratio of infinity) is obtained from Eq. (13) when $d_4/d_2 = d_3/d_1$. The slope of this line is given by $(d_1+d_3)/(d_1-d_3)$. This approximation can give a further reduction of the number of model parameters (to three, d_1, d_2 and d_ρ), at the expense of some loss of accuracy. With only three model parameters the evolution law can be expressed as

$$\dot{\boldsymbol{F}} = \left(\mathrm{tr}(\dot{\boldsymbol{\epsilon}}) - \sqrt{2}\mathrm{tr}(\dot{\boldsymbol{\epsilon}}^{\pi}_{\mathrm{dev}} \cdot \hat{\boldsymbol{\tau}})\right)\left[d_1\hat{\boldsymbol{I}} + d_3\hat{\boldsymbol{\tau}}\right] + d_\rho\dot{\boldsymbol{\epsilon}}^{\rho}\,. \tag{16}$$

6. Concluding remarks

In this study, the (contact-normal) fabric response of two-dimensional, anisotropic granular samples has been investigated by analysing the extensive set of results of DEM simulations of stress probes (Pouragha et al., 2021), considering both coaxial, in-plane as well as non-coaxial, out-of plane probes. Such an investigation is crucial to understanding the behaviour of granular materials under various loading directions. Based on the analysis of the results of DEM simulations, a fabric evolution law (as function of the total strain rate) has been formulated that describes the fabric response of a sample to various loading directions.

It is found that the in-plane and out-of-plane responses are effectively decoupled: the in-plane fabric increment depends only on the in-plane strain increment, while the out-of-plane fabric increment depends only on the out-of-plane strain increment. The out-of-plane fabric increment is proportional to the out-of-plane strain increment, with acceptable accuracy. The in-plane fabric response is found to be linearly dependent on the in-plane strain increment.

A fabric evolution law, Eq. (15), that incorporates these findings has been developed, which accurately describes the fabric response as obtained from the DEM simulations of all probes. The evolution law involves a modest number (five) of parameters. Approximate relations have been formulated that reduce the number of parameters to three or four (at the expense of some accuracy). The model parameters have been determined for a number of samples that correspond to various values of the stress ratio.

The DEM data for the probes and their description by the proposed fabric evolution law Eq. (15) show that when the strain rate is reversed (opposite direction, same magnitude), then the fabric rate is also reversed, *i.e.* $\dot{\boldsymbol{\epsilon}} \rightarrow -\dot{\boldsymbol{\epsilon}}$ implies $\dot{\boldsymbol{F}} \rightarrow -\dot{\boldsymbol{F}}$. However, due to the strongly nonlinear elasto-plastic stress–strain relation (see Fig. 2 (left)), the analogous relation for the stress rate does not hold: $\dot{\boldsymbol{\sigma}} \rightarrow -\dot{\boldsymbol{\sigma}}$ does *not* imply $\dot{\boldsymbol{F}} \rightarrow -\dot{\boldsymbol{F}}$.

Results of the current study that may be valuable in the further development of (three-dimensional) fabric evolution laws that are appropriate for a range of monotonic loading conditions are: (i) the fabric rate is dependent on the total strain rate, (ii) an out-of-plane strain increment results in an out-of-plane fabric response, (iii) the fabric rate is linear in the strain rate and (iv) the term $\mathrm{sym}(\boldsymbol{F}\cdot\dot{\boldsymbol{\epsilon}})$ is important, as follows from the uniform-strain theory in Appendix A.

For the current anisotropic systems, the stress–strain response is incrementally nonlinear (Pouragha et al., 2021) and the fabric-strain response is incrementally linear. This is opposite to the behaviour observed for isotropic systems by Pouragha et al. (2019), where the stress–strain response was incrementally linear ('pseudo-elastic') and the fabric-strain response was incrementally nonlinear (dependent on loading direction). The main factors that may form the origin of this difference in behaviour are considered to be: (i) isotropy vs. anisotropy of the samples, (ii) elastic vs. elasto-plastic stress–strain behaviour, (iii) hydrostatic vs. deviatoric stress state and (iv) employed loading path for creating samples (isotropic compression with varying interparticle friction coefficient for isotropic samples; frictional loading simulation for anisotropic samples). It has been checked that loading rate, probe magnitude, void ratio and linearity of the response during each of the probes are comparable in the studies (Pouragha et al., 2019, 2021). Further analyses are required to exactly pinpoint the most important factor leading to this observed difference in behaviour.

The focus of the current study is on anisotropic, pre-peak samples. For future studies, the behaviour of post-peak samples (especially near the critical state) is very interesting. For such DEM probe studies, it may be more expedient to employ strain probes rather than stress probes, to avoid issues with inaccessibility of some stress states. In addition, the presence of stress fluctuations, caused by the meta-stable stick–slip response (Combe and Roux, 2000) beyond the peak, renders the incremental probing at these states non-trivial. Additionally, the case where the fabric tensor and the stress tensor are *not* coaxial should be considered, to extend the current study where these tensors are coaxial.

Although the presented fabric evolution law accurately describes the fabric response for the considered samples, it cannot (yet) be used in (advanced) constitutive modelling of granular soils for general (or monotonic) loading conditions, since the model parameters (as listed in Table 2) are specific to the samples. Therefore, closed form expressions for the model parameters, as functions of the state vector set $\boldsymbol{S}$ (or combined via the stress ratio q/p and other state variables such as $\psi = e - e_c(p)$), must be formulated. The current data is, however, not sufficient to formulate such closed-form expressions. To accomplish this, additional samples need to be considered, with different void ratios e, mean pressures p, and fabric anisotropy A.

Although the current study focused on two-dimensional systems, the current results provide a sound starting point for studies of evolution laws that account for the influence of loading direction for the deviatoric fabric tensor of physically-realistic three-dimensional systems.

CRediT authorship contribution statement

Chaofa Zhao: Writing – original draft, Methodology, Formal analysis, Software, Data curation, Funding acquisition, Conceptualisation. **Niels P. Kruyt:** Writing – original draft, Methodology, Formal analysis, Data curation, Funding acquisition, Conceptualisation, Validation, Visualisation, Supervision. **Mehdi Pouragha:** Writing – review & editing, Methodology, Software, Formal analysis, Data curation, Funding acquisition, Conceptualisation. **Richard Wan:** Writing – review & editing, Methodology, Funding acquisition, Conceptualisation, Validation, Visualisation, Supervision.

Declaration of competing interest

The authors declare that they have no known competing financial interests or personal relationships that could have appeared to influence the work reported in this paper.

Acknowledgements

The first author acknowledges financial support from the European Union's Horizon 2020 research and innovation program under the Marie Skłodowska-Curie grant agreement No. 832405 (ICARUS). Research funding provided by the Natural Sciences and Engineering Research Council of Canada (RGPIN-2020-06480 and DGECR-2020-00411 held by M. Pouragha and RGPIN-2016-04086 held by R. Wan) is gratefully acknowledged.

Appendix A. Uniform-strain theory for fabric evolution

The fabric tensor in Eq. (4) represents an average of the dyadic product of the normal vectors $\boldsymbol{n}^c$ at contacts. These in turn are determined by the particle positions $\boldsymbol{X}^p$. A basic theory for fabric evolution is obtained from uniform-strain (or affine-deformation) theory, which is employed in many micromechanical theories (for example Bathurst and Rothenburg (1988) and Chang et al. (1995)). In this theory it

is assumed that the displacement $\boldsymbol{U}^p$ of each particle p conforms to the imposed macroscopic strain increment, i.e. $d\boldsymbol{U}^p = d\boldsymbol{\alpha} \cdot \boldsymbol{X}^p$ where $d\boldsymbol{\alpha}$ is the increment of the average macroscopic displacement-gradient tensor. For a vector $\boldsymbol{v}^{AB}$ connecting two points A and B, the uniform-strain assumption for the change $\Delta\boldsymbol{v}^{AB}$ in vector $\boldsymbol{v}^{AB}$ implies that

$$\Delta\boldsymbol{v}^{AB} = \Delta\boldsymbol{\alpha} \cdot \boldsymbol{v}^{AB} \tag{17}$$

Furthermore, it is assumed here that the contact topology is constant, i.e. contacts are neither created nor disrupted. Hence, contact reorientation is the only mechanism of fabric change (Kruyt, 2012) that is accounted for, and hence coordination number Z does not change according to this uniform-strain theory. Employing index notation, it follows from Eq. (4) that

$$\dot{F}_{ij} = \frac{2}{N_p} \sum_{c \in C} \left(\dot{n}_i^c n_j^c + n_i^c \dot{n}_j^c \right) \tag{18}$$

According to the uniform-strain assumption Eq. (17) (with $\boldsymbol{v}^c = \boldsymbol{l}^c$), $\dot{l}_i^c = \dot{\epsilon}_{ij} l_j^c$. Considering a granular system consisting of equal-sized spherical (or disc-shaped) particles and using the definition of the fabric tensor in Eq. (4), it follows that

$$\dot{F}_{ij} = \dot{\epsilon}_{ik} F_{kj} + \dot{\epsilon}_{jk} F_{ki} \equiv 2\mathrm{sym}(\boldsymbol{F} \cdot \dot{\boldsymbol{\epsilon}})_{ij} \tag{19}$$

where $\mathrm{sym}(\boldsymbol{A})$ is the symmetric part of a tensor $\boldsymbol{A}$. Despite all its assumptions (see for example Rothenburg and Kruyt, 2001), the uniform-strain theory is important since it allows to identify an important variable ($\mathrm{sym}(\boldsymbol{F} \cdot \dot{\boldsymbol{\epsilon}})$) for fabric evolution. This theoretical result (that does not require model parameters) in Eq. (19) confirms the finding from DEM simulations in Pouragha (2022) that the *total* strain rate $\dot{\epsilon}_{ij}$, rather than the elastic or the plastic strain rate, is important for the fabric rate.

It should be noted that Eq. (19) does *not* satisfy $\mathrm{tr}(\dot{\boldsymbol{F}}) = \dot{Z} = 0$, even though only contact reorientation is accounted for in the current uniform-strain theory, and hence coordination number should not change. This issue can be resolved in different manners (via some projection operator), but this does not affect the main conclusion of this Appendix that the term $\mathrm{sym}(\boldsymbol{F} \cdot \dot{\boldsymbol{\epsilon}})$ is important for the description of the fabric rate $\dot{\boldsymbol{F}}$.

It is possible to relax some of the restricting assumptions leading to Eq. (19) in order to obtain a relation between strain and fabric that also addresses possible changes in the coordination number (for monotonic loading cases), see Rothenburg and Kruyt (2004), Kruyt (2012) and Pouragha and Wan (2016) for instance.

Appendix B. Dependence of fabric rate on total and plastic strain rates

Here the dependence of the fabric rate on the total strain rate and on the plastic strain rate is shown for the in-plane probes, to graphically show that the total strain rate is the best descriptor of the fabric rate. This was concluded by Pouragha (2022) based on a correlation analysis.

The dependence on the in-plane probe angle ϕ of the norm of fabric increment $\|\Delta\boldsymbol{F}\|$ (determined by Eq. (4)), as well as the norm of the total and the plastic strain increment ($\|\Delta\boldsymbol{\epsilon}\|$ and $\|\Delta\boldsymbol{\epsilon}^p\|$ respectively) are shown in Fig. 8 for the case $q/p = 0.40$. Pouragha et al. (2021) describe how the plastic strains have been determined.

Insignificant plastic deformation is observed for the probes with $0° \leq \phi \leq 60°$ and $255° \leq \phi \leq 360°$, whereas the increment of fabric is significant. Therefore, the plastic strain rate tensor is not the main parameter driving fabric evolution. However, the strain rate tensor is a good descriptor.

Appendix C. Model parameters

The fitted values of the dimensionless model parameters d_1, d_2, d_3, d_4 and d_ρ in the fabric evolution law Eq. (15) are given in Table 2 for the granular samples with various stress ratios q/p. Properties of the samples are given in Table 1.

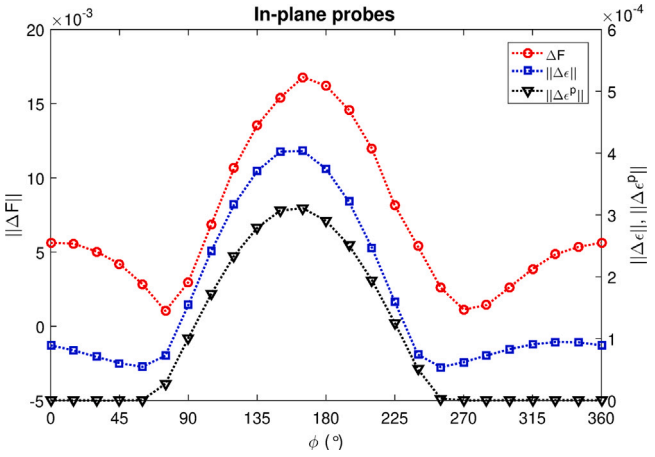

Fig. 8. Norm of fabric increment $\|\Delta\boldsymbol{F}\|$, total strain increment $\|\Delta\boldsymbol{\epsilon}\|$ and plastic strain increment $\|\Delta\boldsymbol{\epsilon}^p\|$ as function of the in-plane probe angle ϕ shown in Fig. 1. Results for in-plane probes for the case of stress ratio $q/p = 0.40$.

Table 2
Variation of the model parameters d_1, d_2, d_3, d_4, d_ρ in Eq. (15) with stress ratio q/p.

q/p	d_1	d_2	d_3	d_4	d_ρ
0.15	51.55	−46.98	−20.05	25.95	24.29
0.30	52.45	−34.97	−20.18	18.30	24.94
0.40	47.20	−22.31	−15.43	15.67	32.20
0.44	42.42	−9.80	−13.12	9.75	28.51

References

Agnolin, I., Roux, J.-N., 2007. Internal states of model isotropic granular packings. II. Compression and pressure cycles. Phys. Rev. E 76 (6), 061303.

Bathurst, R., Rothenburg, L., 1988. Micromechanical aspects of isotropic granular assemblies with linear contact interactions. J. Appl. Mech. Trans. ASME 55, 17–23.

Been, K., Jefferies, M., 1985. A state parameter for sands. Géotechnique 35, 99–112.

Chang, C.S., Chao, S.J., Chang, Y., 1995. Estimates of elastic moduli for granular material with anisotropic random packing structure. Int. J. Solids Struct. 32 (14), 1989–2008.

Christoffersen, J., Mehrabadi, M.M., Nemat-Nasser, S., 1981. A micromechanical description of granular material behavior. J. Appl. Mech. 48, 339–344.

Combe, G., Roux, J.-N., 2000. Strain versus stress in a model granular material: a Devil's staircase. Phys. Rev. Lett. 85 (17), 3628.

Cundall, P.A., Strack, O.D.L., 1979. A discrete numerical model for granular assemblies. Géotechnique 29 (1), 47–65.

Froiio, F., Roux, J.-N., 2010. Incremental response of a model granular material by stress probing with DEM simulations. In: AIP Conference Proceedings. American Institute of Physics, pp. 183–197.

Fu, P., Dafalias, Y.F., 2011. Fabric evolution within shear bands of granular materials and its relation to critical state theory. Int. J. Numer. Anal. Methods Geomech. 35 (18), 1918–1948.

Gao, Z., Zhao, J., Li, X.-S., Dafalias, Y.F., 2014. A critical state sand plasticity model accounting for fabric evolution. Int. J. Numer. Anal. Methods Geomech. 38 (4), 370–390.

Gudehus, G., 1979. A comparison of some constitutive laws for soils under radially symmetric loading and unloading. Can. Geotech. J. 20, 502–516.

Hu, N., Zhuang, P.-Z., Yang, D.-S., Yu, H.-S., 2021. On the evolution law of a contact normal-based fabric tensor for granular materials. Comput. Geotech. 132, 103857.

Imseeh, W.H., Druckrey, A.M., Alshibli, K.A., 2018. 3D experimental quantification of fabric and fabric evolution of sheared granular materials using synchrotron micro-computed tomography. Granular Matter 20 (2), 24.

Karapiperis, K., Harmon, J., Andò, E., Viggiani, G., Andrade, J.E., 2020. Investigating the incremental behavior of granular materials with the level-set discrete element method. J. Mech. Phys. Solids 144, 104103.

Kruyt, N.P., 2012. Micromechanical study of fabric evolution in quasi-static deformation of granular materials. Mech. Mater. 44, 120–129.

Kruyt, N.P., Rothenburg, L., 2016. A micromechanical study of dilatancy of granular materials. J. Mech. Phys. Solids 95, 411–427.

Kruyt, N.P., Rothenburg, L., 2019. A strain–displacement–fabric relationship for granular materials. Int. J. Solids Struct. 165, 14–22.

Kuhn, M.R., 2010. Micro-mechanics of fabric and failure in granular materials. Mech. Mater. 42 (9), 827–840.

Li, X.S., Dafalias, Y.F., 2012. Anisotropic critical state theory: role of fabric. J. Eng. Mech. 138 (3), 263–275.
Li, X., Li, X.-S., 2009. Micro-macro quantification of the internal structure of granular materials. J. Eng. Mech. 135 (7), 641–656.
Oda, M., 1972. Initial fabrics and their relations to mechanical properties of granular material. Soils Found. 12 (1), 17–36.
Oda, M., 1982. Fabric tensor for discontinuous geological materials. Soils Found. 22 (4), 96–108.
O'Sullivan, C., Cui, L., 2009. Micromechanics of granular material response during load reversals: combined DEM and experimental study. Powder Technol. 193 (3), 289–302.
Petalas, A.L., Dafalias, Y.F., Papadimitriou, A.G., 2019. SANISAND-FN: An evolving fabric-based sand model accounting for stress principal axes rotation. Int. J. Numer. Anal. Methods Geomech. 43 (1), 97–123.
Pietruszczak, S., Pande, G.N., 2001. Description of soil anisotropy based on multi-laminate framework. Int. J. Numer. Anal. Methods Geomech. 25 (2), 197–206.
Pouragha, M., 2022. What controls fabric: A correlation analysis for contact fabric evolution in granular media. J. Eng. Mech. 148 (1), 04021121.
Pouragha, M., Kruyt, N.P., Wan, R., 2019. Fabric response to strain probing in granular materials: Two-dimensional, isotropic systems. Int. J. Solids Struct. 156-157, 251–262.
Pouragha, M., Kruyt, N.P., Wan, R., 2021. Non-coaxial plastic flow of granular materials through stress probing analysis. Int. J. Solids Struct. 222-223, 111015.
Pouragha, M., Wan, R., 2016. Strain in granular media: Probabilistic approach to Dirichlet tessellation. J. Eng. Mech. 143, C4016002.
Reynolds, O.C., 1885. On the dilatancy of media composed of rigid particles in contact. Philos. Mag. 20, 469–481.
Rothenburg, L., Bathurst, R., 1989. Analytical study of induced anisotropy in idealized granular materials. Géotechnique 39, 601–614.
Rothenburg, L., Kruyt, N.P., 2001. On limitations of the uniform strain assumption in micromechanics of granular materials. In: Kishino, Y. (Ed.), Powders and Grains 2001. Balkema Publishers, pp. 191–194.
Rothenburg, L., Kruyt, N.P., 2004. Critical state and evolution of coordination number in simulated granular materials. Int. J. Solids Struct. 41 (21), 5763–5774.
Rowe, P.W., 1962. The stress-dilatancy relation for static equilibrium of an assembly of particles in contact. Proc. R. Soc. Lond. Ser. A Math. Phys. Eng. Sci. 264, 500–527.
Rudnicki, J.W., Rice, J., 1975. Conditions for the localization of deformation in pressure-sensitive dilatant materials. J. Mech. Phys. Solids 23 (6), 371–394.
Satake, M., 1978. Constitution of mechanics of granular materials through the graph theory. In: Proceedings of the U.S.-Japan Seminar on Continuum Mechanical and Statistical Approaches in the Mechanics of Granular Materials, Sendai. pp. 47–62.
Schofield, A., Wroth, P., 1968. Critical State Soil Mechanics. McGraw-Hill London.
Shi, J., Guo, P., 2018a. Fabric evolution of granular materials along imposed stress paths. Acta Geotech. 13 (6), 1341–1354.
Shi, J., Guo, P., 2018b. Induced fabric anisotropy of granular materials in biaxial tests along imposed strain paths. Soils Found. 58 (2), 249–263.
Smilauer, V., et al., 2015. Yade Documentation, second ed. The Yade Project, http://dx.doi.org/10.5281/zenodo.34073, http://yade-dem.org/doc/.
Theocharis, A.I., Vairaktaris, E., Dafalias, Y.F., 2017a. Scan line void fabric anisotropy tensors of granular media. Granular Matter 19 (4), 1–12.
Theocharis, A.I., Vairaktaris, E., Dafalias, Y.F., Papadimitriou, A.G., 2017b. Proof of incompleteness of critical state theory in granular mechanics and its remedy. J. Eng. Mech. 143 (2), 04016117.
Theocharis, A.I., Vairaktaris, E., Dafalias, Y.F., Papadimitriou, A.G., 2019. Necessary and sufficient conditions for reaching and maintaining critical state. Int. J. Numer. Anal. Methods Geomech. 43 (12), 2041–2055.
Thornton, C., 2000. Numerical simulations of deviatoric shear deformation of granular media. Géotechnique 50 (1), 43–53.
Thornton, C., Barnes, D.J., 1986. Computer simulated deformation of compact granular materials. Acta Mech. 64, 45–61.
Tsuchikura, T., Satake, M., 2001. A consideration on the statistical analysis of particle packing using loop tensors. In: Powders and Grains 2001. Swets & Zeitlinger, pp. 29–32.
Viggiani, G., Tengattini, A., 2019. Recent developments in laboratory testing of geomaterials with emphasis on imaging. In: Proceedings of the XVII European Conference on Soil Mechanics and Geotechnical Engineering, Reykjavík, Iceland.
Wang, R., Dafalias, Y.F., Fu, P., Zhang, J.-M., 2020. Fabric evolution and dilatancy within anisotropic critical state theory guided and validated by DEM. Int. J. Solids Struct. 188–189, 210–222.
Wang, R., Fu, P., Zhang, J.-M., Dafalias, Y.F., 2017. Evolution of various fabric tensors for granular media toward the critical state. J. Eng. Mech. 143 (10), 04017117.
Wiebicke, M., Andò, E., Viggiani, G., Herle, I., 2020. Measuring the evolution of contact fabric in shear bands with x-ray tomography. Acta Geotech. 15 (1), 79–93.
Yang, Z.X., Li, X.S., Yang, J., 2008. Quantifying and modelling fabric anisotropy of granular soils. Géotechnique 58 (4), 237–248.
Yang, Z.X., Wu, Y., 2016. Critical state for anisotropic granular materials: a discrete element perspective. Int. J. Geomech. 17 (2), 04016054.
Yang, Z.X., Xu, T.T., Chen, Y.N., 2018. Unified modeling of the influence of consolidation conditions on monotonic soil response considering fabric evolution. J. Eng. Mech. 144 (8), 04018073.
Yoshimine, M., Ishihara, K., Vargas, W., 1998. Effects of principal stress direction and intermediate principal stress on undrained shear behavior of sand. Soils Found. 38 (3), 179–188.
Zhao, J., Guo, N., 2013. Unique critical state characteristics in granular media considering fabric anisotropy. Géotechnique 63 (8), 695–704.
Zhao, C.-F., Kruyt, N.P., 2020. An evolution law for fabric anisotropy and its application in micromechanical modelling of granular materials. Int. J. Solids Struct. 196–197, 53–66.
Zhao, C.-F., Pinzón, G., Wiebicke, M., Andò, E., Kruyt, N.P., Viggiani, G., 2021. Evolution of fabric anisotropy of granular soils: x-ray tomography measurements and theoretical modelling. Comput. Geotech. 133, 104046.